Vision Res. Vol. 29, No. 2, pp. 223–240, 1989
Printed in Great Britain.

0042-6989/89 $3.00 + 0.00

FUNCTIONAL ANATOMY OF NORMAL HUMAN RECTUS MUSCLES

JOEL M. MILLER
Smith-Kettlewell Eye Research Institute, 2232 Webster Street, San Francisco, CA 94115, U.S.A.

(*Received* 25 *January* 1988; *in revised form* 3 *June* 1988)

Abstract—The actions of extraocular muscles depend on their positions as a function of gaze. These positions vary with muscle forces, which are normal only in alert subjects making voluntary fixations.

Magnetic Resonance Imaging (MRI) was used to view normal human orbits, with voluntary gaze varied over a circular field 77 deg in dia, centered on the orbital axis. Computer-aided reconstructions, reflecting the data of four normal adult subjects, produced clear pictures of the rectus muscles and optic nerve, and yielded data on muscle paths and cross-sections.

From their origins in the orbital apex to their points of tangency with the globe, rectus muscle side-slip, relative to the orbit, is approximately zero; consequently, their "muscle planes" (though not necessarily their axes of rotation) are approximately fixed in the orbit. As the rectus muscles contract they draw in towards the orbital axis, and as they relax they bow outwards; this excursion is as large as 3.7 mm. Contraction also tends to cause the planes of maximum cross-section to move posteriorly.

Extraocular muscle Human MRI Muscle plane Muscle side-slip NMR
Ocular model Ocular statics Optic nerve Orbital geometry

INTRODUCTION

Studies of fixed specimens (e.g. Koornneef, 1983; Nakagawa, 1965; Volkmann, 1869) do not provide a sufficient anatomic basis for understanding the actions of eye muscles. As we have argued previously (Miller and Robinson, 1984; Miller and Robins, 1987), muscle paths are a function of innervations, as well as of various elasticities and gaze position. They must, therefore, be determined in alert subjects during voluntary fixation.

It is convenient to define a left-handed Cartesian coordinate system, u-v-w, with origin at the geometric center of the globe, w-axis aligned with the axis of symmetry of the orbital cone and pointing forward, and v-axis pointing upward (see Fig. 1). A muscle's path may be defined for our purposes by the line, p connecting the area centroids, C, of its cross-sections parallel to the plane, u-v. We will be concerned with two directions of movement of points on this path. The first is *radial* movement, r, which is towards or away from the axis of the oribital cone, w. The second is *sideways* movement or *side-slip*, s, which is perpendicular to the path and to the radial direction. As shown in Fig. 1, with the head erect, side-slip of the lateral rectus would move it up and down along the surface of the globe.

In the absence of muscle path data from alert subjects, ocular modeling and surgical planning have proceeded on untested assumptions about how the orbital contents behave when the eye moves. The simplest model assumption is the "shortest path" hypothesis (Krewson, 1950; Boeder, 1962), according to which the muscles may slip freely across the globe; because they are under tension, they would then always take the shortest path, which on a sphere is a great-circle. However, for gazes within the normal range, shortest path models predict large amounts of side-slip, leading to gross rearrangements of the muscles, which certainly do not occur. The "permitted side-slip" model of Robinson (1975) eliminates these catastrophic effects by placing certain geometric constraints on side-slip. A refinement of this analysis, which modeled the side-slip forces due to intermuscular tissues and muscle tensions, was done by Miller and Robinson (1984).

Research-oriented models of 3-dimensional eye movements tend to assume the numerical results of current permitted side-slip models (e.g. Robinson, 1985; Miller and Robins, 1987; Kault *et al.*, 1987). Clinical students of ocular motility, however, need practical models, simple enough to use mentally in support of clinical judgements. A common clinical assumption has

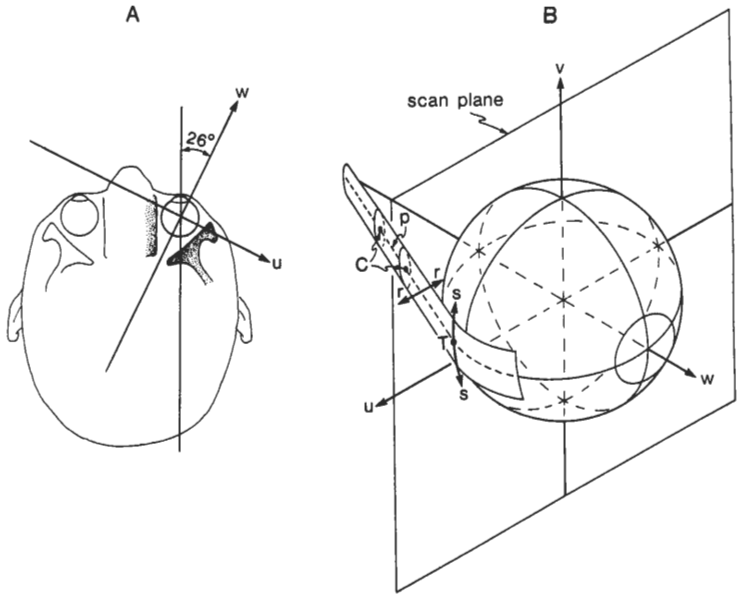

Fig. 1. Coordinates and movement directions. (A) Schematic view of the subject's head from above, showing the orientation of the u-v-w coordinate system with respect to the straight-ahead direction. (B) The globe and lateral rectus pictured in the u-v-w coordinate system, with gaze along the axis of symmetry of the orbital cone (w). The muscle's path, p, is shown as the line connecting the area centroids, C, of slices parallel to the u-v scan plane. Sideways movement of the point of tangency of muscle with globe, T, is indicated by the arrows labeled s. Radial movement of a point on the muscle path is indicated by the arrows labeled r.

been that the muscle planes* remain fixed in the orbit (see e.g. Scott, 1983). This assumption is incompatible with the shortest path hypothesis; however, it can be modeled with appropriate choices of the parameters of a permitted side-slip model.

In an earlier study, we collected data on the functional anatomy of the orbit, using conventional x-ray imaging of radio-opaque sutures implanted in the lateral rectus muscles of monkeys trained to fixate (Miller and Robins, 1987). In that study we found that, over much of its length, the lateral rectus (LR) remained roughly stationary relative to the orbit, as the eye moved through a ± 25 deg horizontal and vertical range. In particular, the mechanically important point of tangency of the muscle with the globe (point T in Fig. 1) remained almost stationary with respect to the orbit. That study was limited, however, to the LR muscle and to monkeys. Further, the implantation surgery produced some scarring around the LR.

x-Ray CT scans are useful for viewing eye muscles. However, because orbital structures, particularly the lens, may be damaged by ionizing radiation, only fragmentary data can be collected by this method. Still, some suggestive results have been obtained with single-slice CT scans. Following our suggestion, Simonsz *et al.* (1985) performed CT scans in a plane perpendicular to the orbital axis and just behind the globe, as subjects fixated, in turn, primary position and four 30 deg eccentric secondary positions. A horizontal scan that included the horizontal recti was also performed for primary, adducting and abducting gaze positions. It was found that there was no consistent side-slip of the horizontal recti with vertical movement, or of the vertical recti with horizontal movement. The antagonist of each pair of recti was found to curve outward in secondary positions.

The ideal method for studying the functional anatomy of the orbit would be fast, non-invasive, able to differentiate sclera, tendon, muscle, fat and bone, have an isotropic spatial resolution of a fraction of a mm, and be safely applicable to any subject population. Current Magnetic Resonance Imaging (MRI) satisfies most of these criteria. Its weaknesses in our application are its somewhat low speed (considering that the subject must maintain fixation during the scan), the difficulty distinguishing

*A muscle plane is determined by a muscle's origin, its point of tangency with the globe and the center of rotation of the globe.

sclera from tendon and its poor resolution in planes perpendicular to the scan plane.

METHODS

MRI scanning

The MRI device used in this study was a Siemens Magnetom with a 0.5 Tesla magnet, located at Pacific Presbyterian Medical Center.

Resolution. Useful spatial resolution depends on the scanning time per orbital image and the MR signal-to-noise ratio.

Imaging a slice with an $n \times n$ matrix of picture elements (pixels) requires n excitations of that slice, each followed by signal sampling or acquisition. Excitation reduces the tissue's longitudinal magnetization, requiring a minimum of about 0.5 sec between excitations to allow the tissue magnetization to realign with the main field. The excitation and sampling itself takes about 100 msec (independent of the number of pixels), allowing us to excite and sample other slices in the interim. We collected 15 slices in such an interleaved fashion with a "repeat time" (TR) of 1.5 sec. For resolution of 256 × 256 pixels, 256 excitation–acquisition cycles would have been required, for a time of 6.4 min to image the whole orbit in one gaze position. We determined experimentally that holding eccentric fixation for 6.4 min was unpleasant, and that fatigue-related movements and fixation errors tended to efface the high resolution expected. We therefore settled on a resolution of 128 × 128 pixels and a scan time of 3.2 min per gaze position.

We defined the region to be imaged by increasing the magnetic gradients in the slice plane while keeping the sampling bandwidth fixed. The strongest gradient available on our machine selects a 15 cm square region of tissue, so that each pixel in the 128 × 128 matrix represented a 1.2 mm square of tissue.

Slice thickness, the third dimension of the tissue volume reflected in a pixel, was chosen to be 3 mm, the minimum available on our machine. By using contiguous slices, the 15 slices we collected spanned a 45 mm distance along the w axis (Fig. 1).

As resolution increases, the volume of tissue contributing to each pixel in the image decreases, and the signal-to-noise ratio drops, causing the individual pixels to become less reliable. To improve the signal-to-noise ratio we used a *surface coil*, which samples the MR signal close to the region of interest.

Instrument calibration. The MRI scanner is well suited to quantitative studies. There are two types of calibration errors of concern: a scale error for each spatial coordinate, and errors due to nonlinearities. Scale calibration uses a standard target, a cylinder of coppper nitrate of known dimensions. Adjustments can be made in all three coordinates to the limit of resolution of the imaging system (0.6 mm), which amounts to a 0.4% error. In routine practice scale errors remain within 1%. We assume this latter value, since the instrument was not specially calibrated for our use. Nonlinearities in the image are due to inhomogeneities in the magnetic fields. The static inhomogeneities are typically 0.003% over a 50 cm dia. spherical region around the center of the magnet. More important are dynamic inhomogeneities caused by eddy currents generated by the gradient pulses. These can lead to scale distortions as large as 10%, far from the center of the magnet. Within the "head region", however, linearly is better than 3%. Our measurements, confined to the orbit, are at least this linear. None of these errors is large enough to be of concern in the present study.

Subjects

Subjects were four adult Caucasian males, between 25 and 40 yr-old, with normal uncorrected vision and ocular motility.

None of the subjects had metallic or electronic implants that might be affected by the scanner's electromagnetic fields. All gave written informed consent.

Data collection

Each subject lay supine on the scanner table (see Fig. 2). The dominant eye (determined by a sighting dominance test) was chosen for fixation, and the head was turned about 26 deg away from the chosen eye. The subject's other eye was patched to prevent diplopia and alternating fixation. The surface coil was positioned horizontally, and as close to the orbit as possible to maximize signal strength. Close placement also maximized the subject's field of view through the coil's circular aperture, allowing as large a range of fixation as possible. To obtain as close to a cross-sectional view as possible of all of the rectus muscles and optic nerve, we adjusted the head turn until the orbital axis was oriented vertically in the transaxial plane, based on transaxial scans at the level of the outer canthi. As we suggested above, optimizing the scanning planes for the recti precluded obtain-

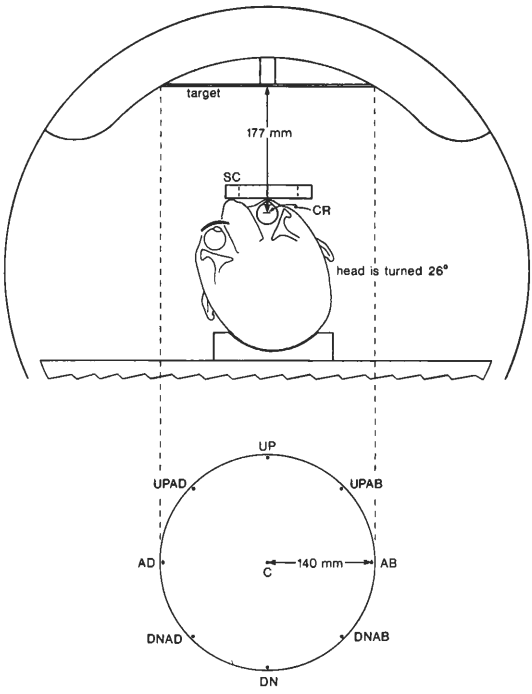

Fig. 2. Positions of the subject and fixation targets. The upper part of the figure schematically shows the view along the axis of the magnet from above the supine subject's head. The head was turned leftward about 26 deg and tilted in pitch to make the axis of the orbital cone of the measured (here, the right) eye vertical. The surface coil (*SC*) was positioned horizontally above the measured eye and as close as possible to it. The fixation targets, drawn on a cardboard disk (*target*) stuck to the inside of the magnet, were viewed through the open center of the surface coil. The lower part of the figure shows the nine targets as seen by the subject. The distance between the center of rotation of the eye (*CR*) and the central fixation target (*C*) was 177 mm. The remaining targets were spaced as shown, each 140 mm from target *C*. The fixation targets are referred to by gaze direction as follows: *C* = central, *UP* = upward, *UPAB* = upward and abducting, *AB* = abducting, *DNAB* = downward and abducting, *DN* = downward, *DNAD* = downward and adducting, *AD* = adducting, *UPAD* = upward and adducting.

ing good data on the inferior oblique and the tendon of the superior oblique, which were therefore excluded from study.

Centered about the orbital axis of the seeing eye was an array of fixation targets drawn on paper and affixed to the inside of the magnet. Limited space forced us to put the targets rather close to the subject, about 18 cm from his eye's center of rotation. It was important to control head position, both to achieve a sharp image and to be able to infer the position of the eye in the head from its position in space. Effective stabilization was achieved by resting the head on a moulded pillow, and wedging foam-rubber blocks between the sides of the head and specially-constructed lateral supports.

Each fixation target was a black dot in the center of a 3 mm dia. bright orange circle on white paper. This target produced a strong afterimage, which could be seen against the white paper if the eye wandered, providing the subject with feedback about fixation accuracy. Sufficiently accurate fixation in primary position for many minutes was not difficult to achieve. In nonprimary gaze positions fixation could be adequately maintained for the 3.2 min required. A central target was aligned with the orbital axis, and eight peripheral targets were equally spaced on a 140 mm radius circle around the central target (see Fig. 2).

The scan data for subject JM in the UPAB gaze position was inadvertently lost.

Data analysis

To improve the reliability and generality of our results, we wanted to produce an image that combined the scan data of all four of our subjects. However, we knew of no well-defined method for "averaging" arbitrary 3-dimensional objects. Fortunately, our inter-subject differences were small, and the rectus muscles and optic nerve were each roughly cylindrical, without multiple abrupt changes in cross-section. These circumstances made it possible to design methods for combining data, which were found to reasonably summarize the data of the individual subjects (see below).

The digitizing, normalizing, and combining

Fig. 3. A set of scans showing subject JM fixing the central target. Slices are each 3 mm thick and perpendicular to the orbital axis *w*. In each image, left is medial, right is lateral, up is superior, and down is inferior. The upper-left slice is most posterior, and the lower right most anterior. The rectus muscles and the globe or optic nerve show clearly as dark structures against the bright orbital fat. The superior oblique muscle is also visible against the orbital wall in the superior-medial quadrant of most slices, although we did not concern ourselves with it. The difficulty in partitioning the superior rectus-levator complex is apparent in most slices. In the two most anterior slices, the dense lateral levator aponeurosis (LLA) obscures the superior margin of the lateral rectus and the lateral margin of the SR, although with the superior contrast of the orginal film these can be discerned. (IR = inferior rectus; LR = lateral rectus; Lev = levator palpebrae superioris; MR = medial rectus; ON = optic nerve; OW = orbital wall; SO = superior oblique; SR = superior rectus.)

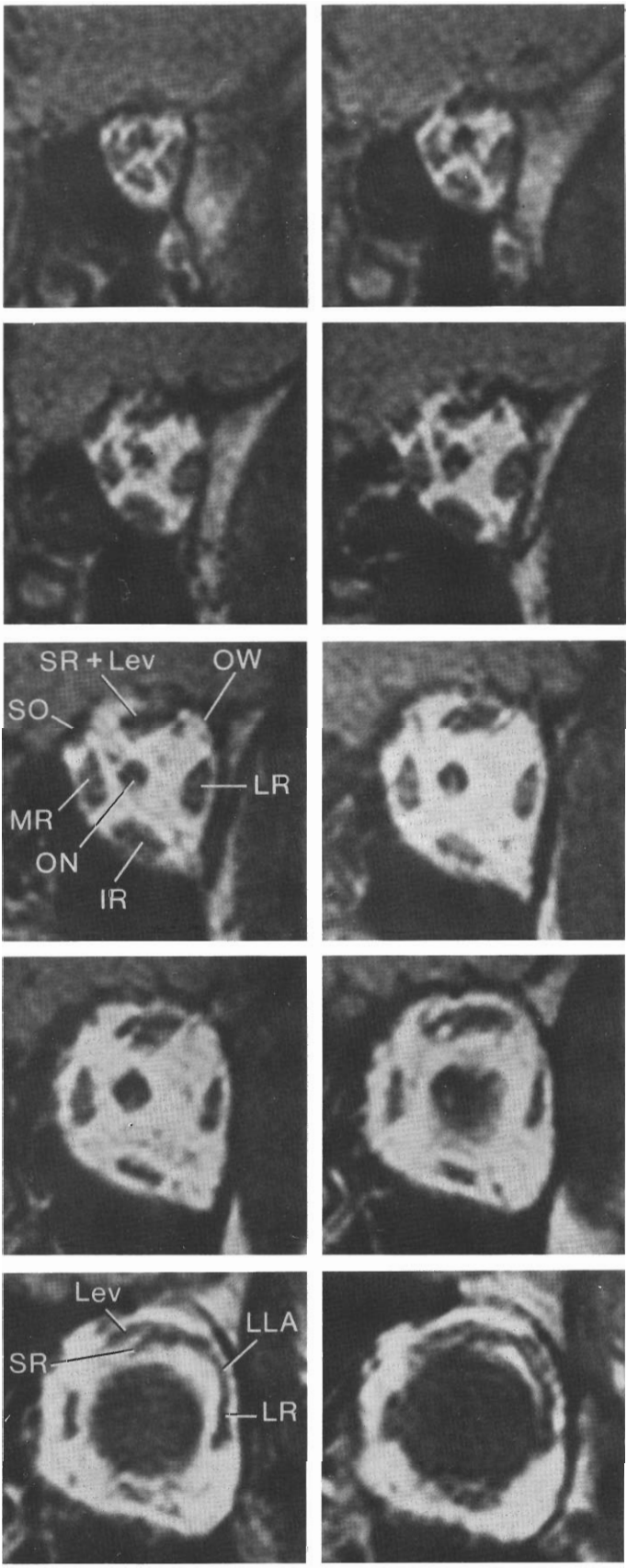

Fig. 3. *Caption on facing page.*

operations described below were performed with custom software and Unix* utilities.

Digitization. Slice data came from the scanner on the usual radiographic film (see Fig. 3). Our consulting radiologist reviewed the films, and defined the contours of the orbital wall, globe or optic nerve, and rectus muscles, in pencil on each slice image. We then traced these contours on a digitizing pad (Houston Instruments Hipad) connected to a lab computer (Masscomp MC-5500). For each of four subjects, and each of nine gaze positions, we digitized between 9 and 12 slices for each of the structures of interest.

We were not able to digitize all the images we collected. In the posterior direction, the reduction in orbital fat made it difficult to discriminate the structures of interest. Therefore, cross-sectional area data for the posterior regions of the muscles were not available. Anteriorly, it was difficult to discriminate tendonous muscles from sclera at, and anterior to, their points of tangency. The absence of contrasting fat separating these structures, and the difficulty in discriminating tendon from sclera, was compounded by the increased density of connective tissue in the anterior orbit. In particular, the lateral levator aponeurosis tended to obscure the superior margin of the lateral rectus and the lateral margin of the superior rectus (see Fig. 3).

It was difficult to distinguish in our scans the superior rectus (SR) from the levator palpeabre, especially in posterior slices. Our division of the SR-levator complex was sometimes arbitrary, and certain of our data for the SR was therefore judged unreliable.

Normalization. Each data set was transformed, if necessary, to the orientation of a right eye.

Head positions of the four subjects differed somewhat, requiring certain transformations to bring them into alignment. Some transformations were based on orbital contents, and so resulted in loss of information about these contents. Other transformations were based on the orbital walls, and so did not have this problem.

To standardize the rotational orientation of the data about the axis of the orbital cone (w in Fig. 1), we viewed the data for the orbital walls and rectus muscles along that axis. For each subject we estimated a single rotation about the axis of the orbital cone that would best align his data with that of the other subjects. By attributing these inter-subject differences to uncontrolled head position we discarded information about true inter-subject differences in the arrangement of the muscles about the orbital axis. Such data is available elsewhere (Saunders *et al.*, 1986). Note that this procedure did not lose information concerning *changes* in muscle position with gaze.

For each gaze position, the data of the four subjects were translated along the oribital axis, aligning the globe-to-optic nerve transition. Information about globe translation was consequently lost.

From displays of the orbital walls in lateral and superior views, we calculated the rotations and translations needed to align the four samples of each gaze position from these points of view.

To combine the data of the four subjects, all samples had to span the same range on the orbital axis. We truncated samples that extended farther than the others in either anterior or posterior directions. In a few cases, we extrapolated an unusually short sample. The resulting data extended along the orbital axis from a point 19 mm posterior to a point 5 mm anterior to the junction of the globe and optic nerve.

To display cross-sectional areas we then resliced the data of each subject perpendicular to the orbital axis w at 2 mm intervals. (Although these are not true cross-sections of the individual structures we will, for brevity, refer to them as such). These cross-sectional areas were then plotted as Fig. 4.

Combination and rendering. Each normalized sample was resliced perpendicular to the orbital axis at 0.5 mm intervals, and each of the resulting closed contours represented by the points on it in 16 equally-spaced directions from the contour's area centroid. Points were ordered to be correlated across subjects. Thus, the problem of combination was reduced to that of combining two-dimensional closed contours. For each contour, then, we subtracted its area centroid from each point, and averaged the X and Y coordinates across each set of four corresponding points. Finally, we added the mean centroid to each mean contour point. The result was an array of points describing the surfaces of the four rectus muscles, and the globe and optic nerve of an "average" eye.

*Trademark of Bell Laboratories.

To represent muscle position and evaluate its changes we resliced the average eye at 1 mm intervals, and computed the area centroids for each slice (Figs 5 and 6).

Finally, to provide an overall picture of the orbital contents, we used the Unigrafix (Séquin, 1983) *ugdisp* rendering program to produce 3-dimensional representations of the combined data in parallel projection, which were then redrawn by our medical illustrator (Fig. 7).

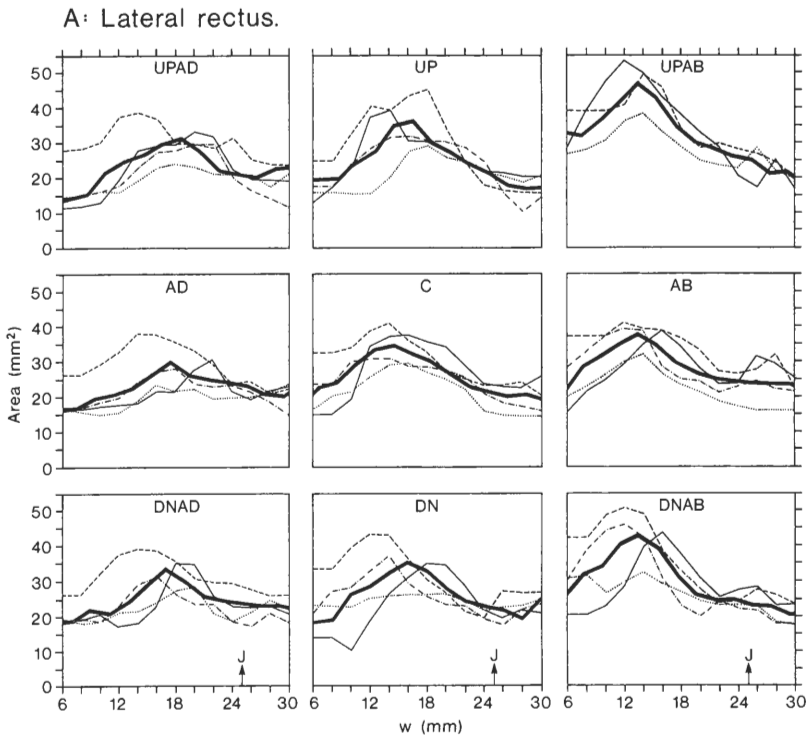

Fig. 4A

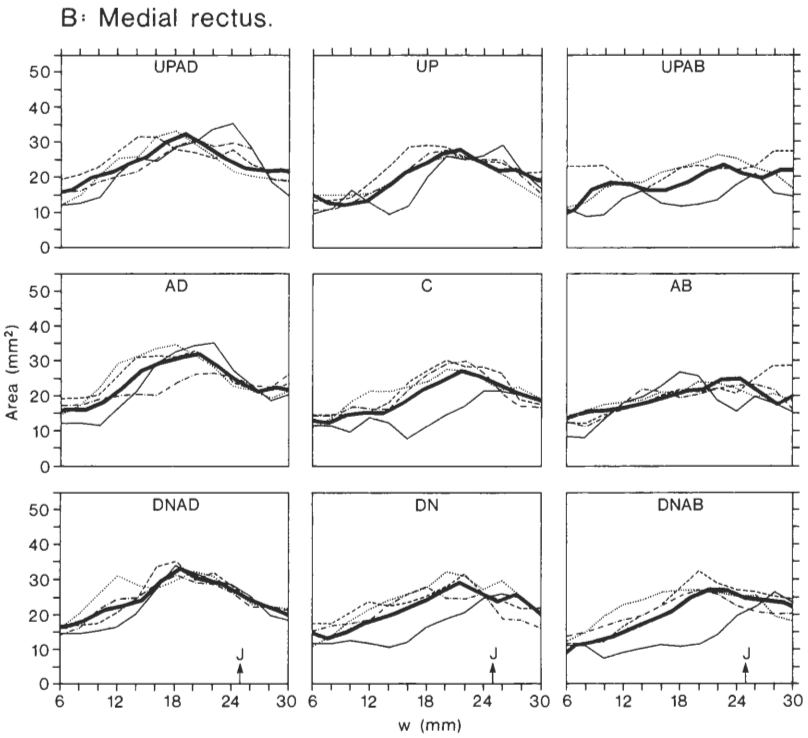

Fig. 4B

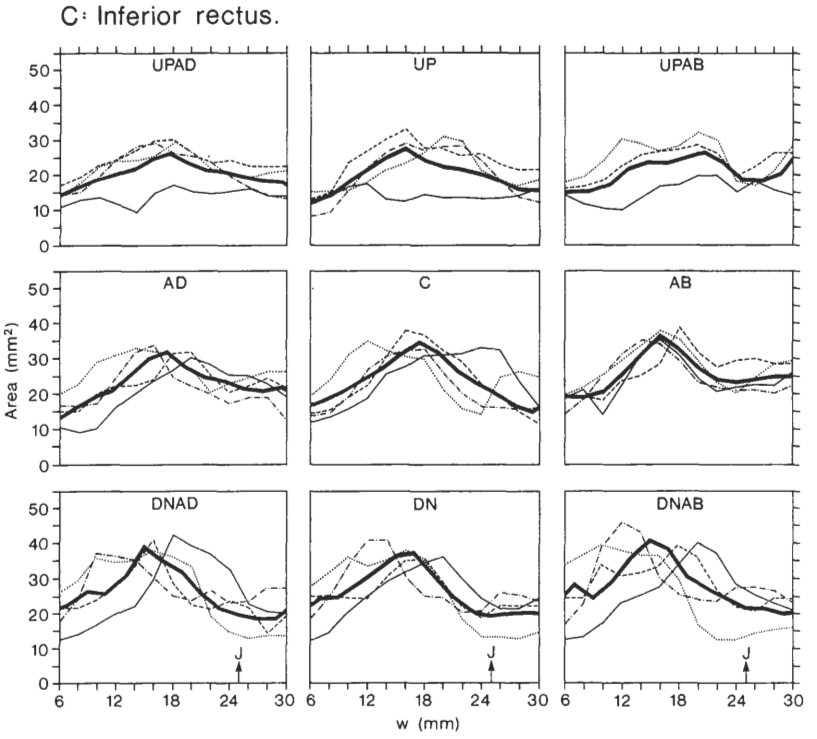

Fig. 4C

Fig. 4. Muscle cross-section areas at different gaze positions for three rectus muscles. Gaze positions UPAD, UP, etc. are as described in Fig. 2. In each panel, the abscissa gives position along the orbital axis (w) in mm; the position marked by the small arrow labeled J is the junction of the globe and optic nerve. The dot-dashed, thin-solid, dotted and dashed lines represent the data of subjects JM, KM, TN and BS, respectively. The thick solid lines represent "mean" data, as explained in the text.

RESULTS

Cross-sectional areas

Figure 4 shows the areas of cross-sections of the rectus muscles for all subjects. At gaze position C the eye is aligned with the orbital axis; each of the other gaze positions is 38 deg eccentric from C, as shown in Fig. 2. In the graph for each gaze position the abscissa is the position of the slice along the orbital axis (w) in mm; the junction of the globe and optic nerve is arbitrarily set to be 25 mm (small arrow labeled J on abscissa), which puts the apex of the orbit at about 1.5 mm (off the axis of Fig. 4). Each thin-line curve represents the data of one subject. The mean location of the maxima of these curves was found, and each curve was translated along the w axis to align its maximum with the mean. The mean of the curves so translated is shown as the thick-line in each panel of Fig. 4; both coordinates of its peak are means of the respective coordinates of the peaks of the curves for individual subjects. It can be seen from Fig 4A and B that in up-gaze, level-gaze, and down-gaze, as the eye rotates into the fields of action of the lateral and medial recti, these muscles thicken, and their thickest parts tend to move posteriorly. Figure 4C shows similar effects for the inferior rectus as the eye moves into its field of action.

For the lateral rectus (LR), as the eye rotates from the AD to the AB gaze position (77 deg) the mean increase in maximum cross-section is 27%; in rotating from UPAD to UPAB (52 deg) the mean increase is 49%; from DNAD to DNAB (52 deg) it is 30%. The overall mean increase in LR maximum cross-section is 35%. Of the 23 comparisons available (2 movements in each of 3 vertical positions for each of 4 subjects, less 1 due to missing data), 20 show increased maximum cross-sections for movements into the LR's field of action. The three "horizontal" rotations, AD to AB, UPAD to UPAB, and DNAD to DNAB, move the point of maximum cross-section posteriorly 4, 5, and 3.5 mm, respectively, for an average of 4.2 mm. Seventeen out of 23 comparisons support this pattern. Only small and inconsistent changes to the LR occur with "vertical" rotations (DN to UP, DNAD to UPAD, DNAB to UPAB).

Changes in the maximum cross-section of the medial rectus (MR) are similar to those of the LR: 30% from AB to AD, 38% from UPAB to UPAD, and 21% from DNAB to DNAD, for a mean increase of 30% (supported by 17 out of 23 comparisons). The corresponding posterior movements of the points of maximum cross-section are 3, 3.5 and 3.5 mm, for an average of 3.3 mm (supported, however, by only 14 out of 23 comparisons).

Data for the inferior rectus (IR) are shown in Fig. 4C. As the eye rotates from the UP to the DN gaze position (77 deg) the mean increase in the maximum cross-section of the inferior rectus (IR) is 35%; in rotating from UPAD to DNAD (52 deg) the mean increase is 48%; in rotating

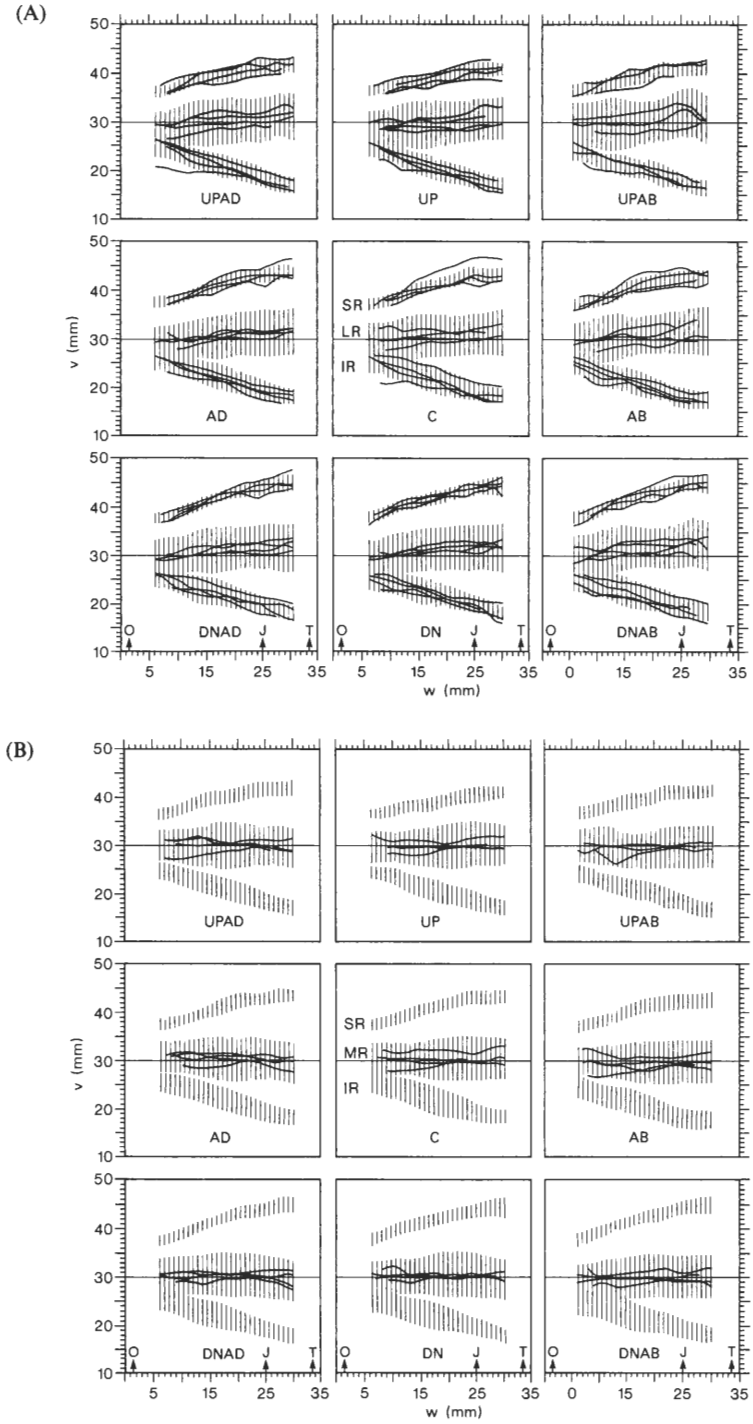

Fig. 5A, B

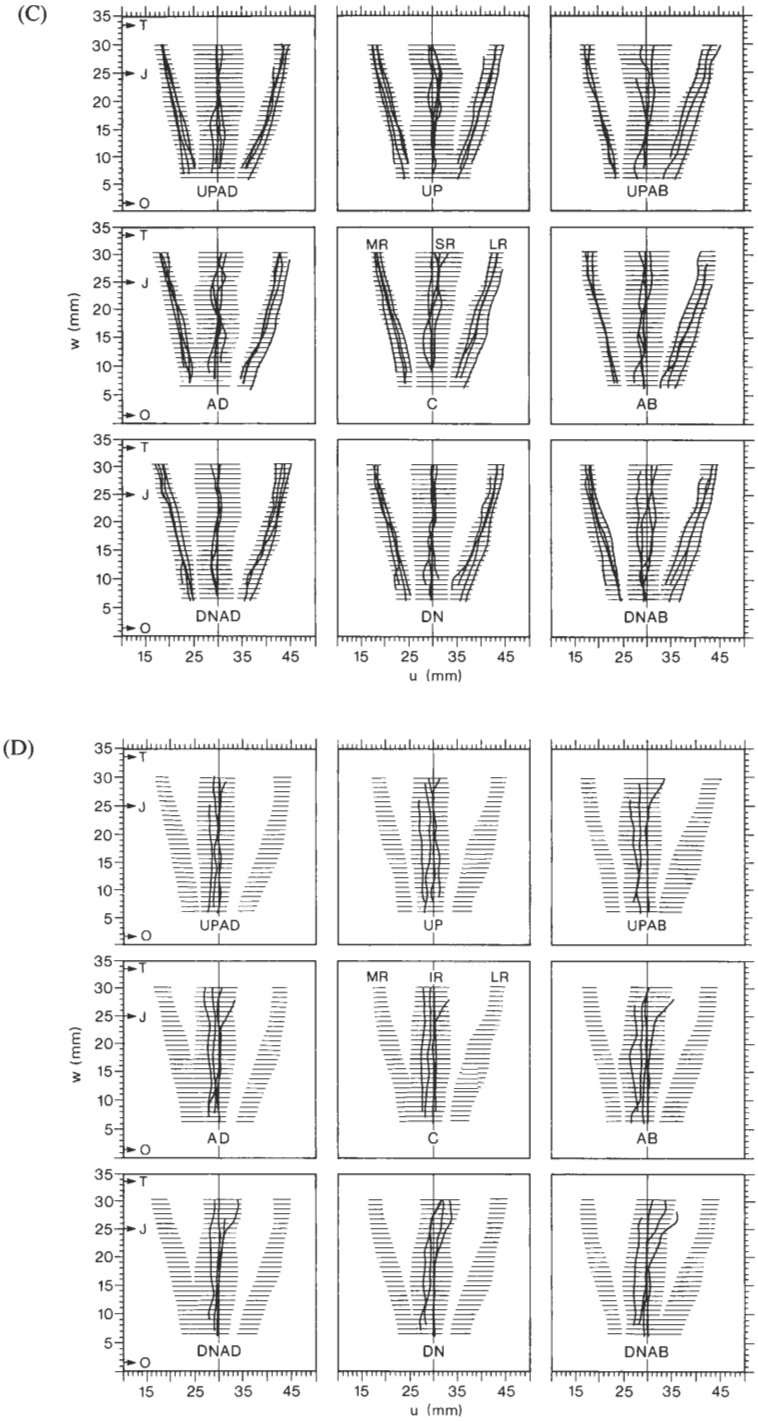

Fig. 5C, D

Fig. 5. Rectus muscle positions. Each panel shows three rectus muscles in either side or top view. (The centered horizontal lines in each side view indicates the slice plane of the top views, and the centered vertical line in each top view indicates the slice plane of the side views.) Each shaded band represents the muscle synthesized from the combined data of all the subjects. The associated solid wiggly lines each connect the area centroids of the slices of one subject. The arrows labeled *O* and *T* indicate the estimated positions along the orbital axis of the muscle origins and the points of tangency of the muscles with the globe, respectively. The arrows labeled *J* show the position of the junction of the globe and optic nerve. (A) Side view of SR, LR and IR. (B) Side view of SR, MR and IR. (Per-subject data for SR and IR are already shown in Fig. 5A; only the synthesized data are repeated for reference.) (C) Top view of MR, SR and LR. (D) Top view of MR, IR and LR. (Per-subject data for MR and LR is available in Fig. 5C.)

from UPAB to DNAB (52 deg) the mean increase is 54%. The overall mean increase in IR maximum cross-section is 46% (supported by 22 out of 23 comparisons). The corresponding posterior movements of the points of maximum cross-section are −1, 2.5 and 4.5 mm, for an average of 2.0 mm (supported, however, by only 12 out of 23 comparisons).

The cross-section data for the SR were unreliable, and are, therefore, not reported (see Methods).

Positions of the muscles

In Fig. 5 both the combined data and the data of individual subjects are presented, exhibiting the mean positions of the muscles as a function of gaze, and the variation across subjects in those positions.

Each shaded band is a view of a muscle synthesized, as described above, from the data of all subjects. Associated with some bands are groups of wiggly lines; each line connects the area centroids of the slices of that muscle for a single subject.

Our data cover the middle part of each muscle (see Methods). About 4.5 mm of muscle is not resolved from the muscle origin (arrow *O*) to the most posterior section. The length of muscle and tendon not resolved, from the muscle insertion to the most anterior section, is estimated to be 12 mm for the LR, 16 mm for the MR and 14 mm for the SR and IR, in gaze position *C*. The junction of the globe and optic nerve (arrow *J*) is at 25 mm on the *w* axis (see Fig. 1), placing the center of the globe at about 37 mm on this axis (off the graph). The point of tangency of muscle with globe is at about 33.5 mm for all muscles and gaze positions (arrow *T*).

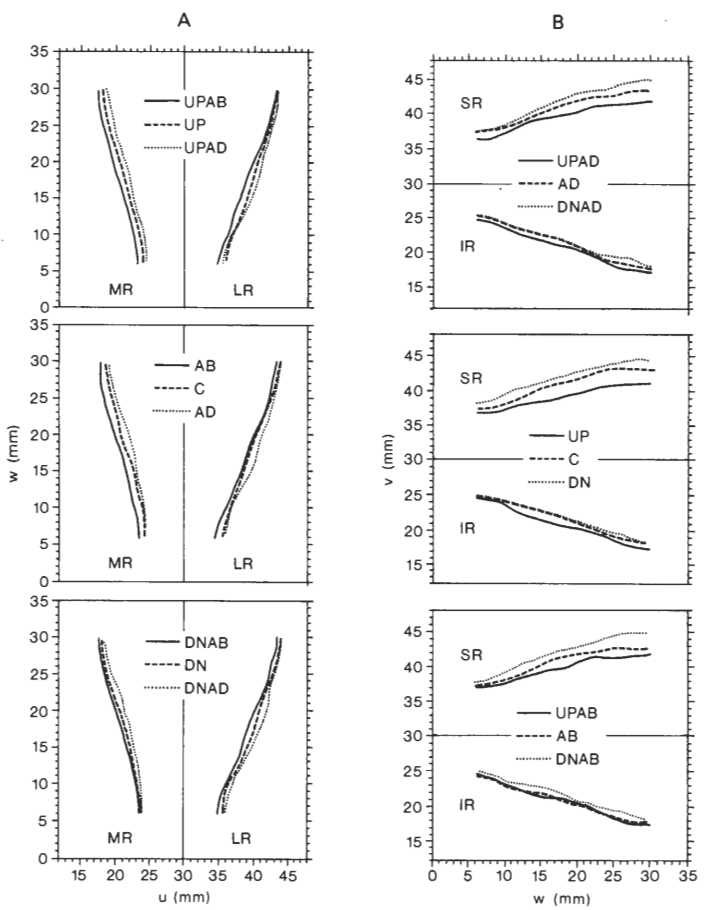

Fig. 6. Centroids of muscles from combined data of all subjects. (A) Top view of LR and MR. Top panel shows the up-gaze positions: UPAB (solid line), UP (dashed), and UPAD (dotted); middle panel shows the level-gaze positions: AB (solid), C (dashed), and AD (dotted); botom panel shows the down-gaze positions: DNAB (solid), DN (dashed), and DNAD (dotted). (B) Side view of SR and IR. Top panel shows the adducted positions: UPAD (solid), AD (dashed), and DNAD (dotted); middle panel shows: UP (solid), C (dashed), and DN (dotted); bottom panel shows the abducted positions UPAB (solid), AB (dashed), and DNAB (dotted).

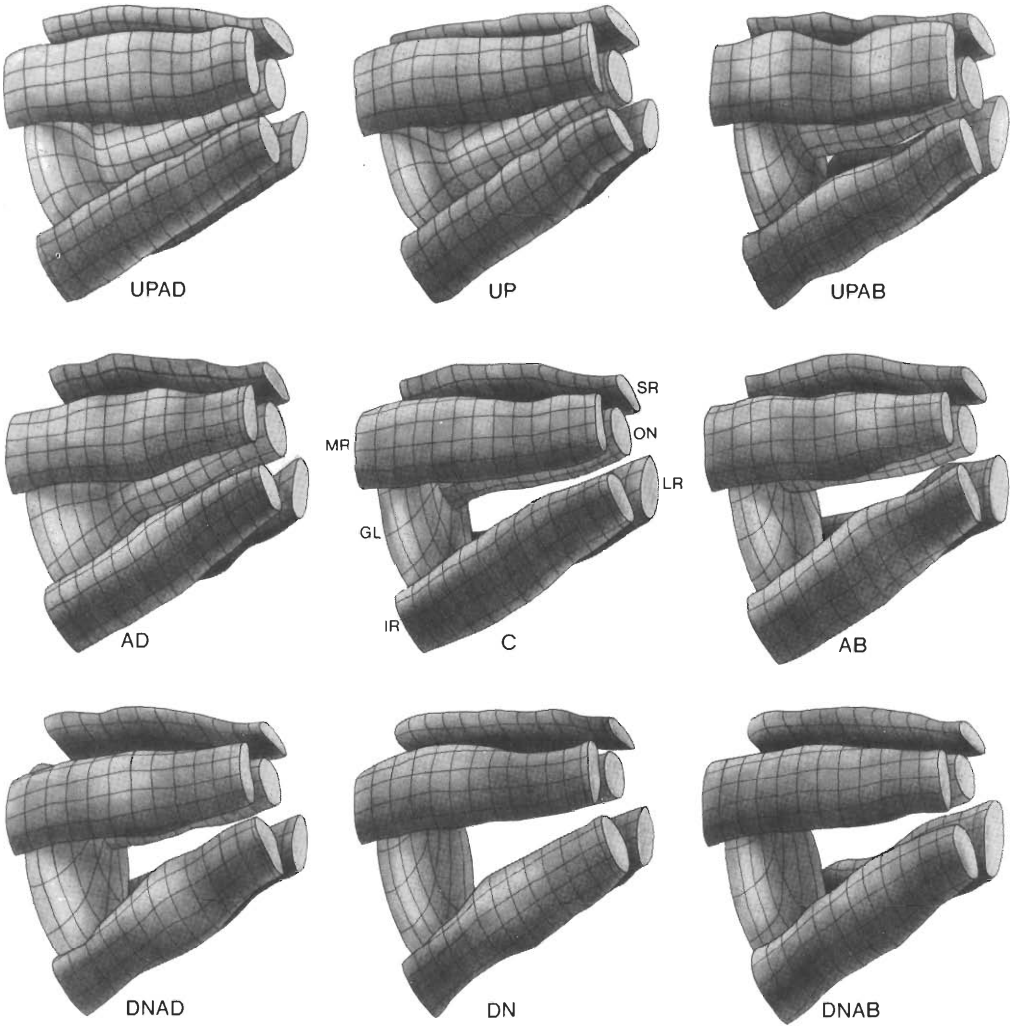

Fig. 7(A). *Caption overleaf.*

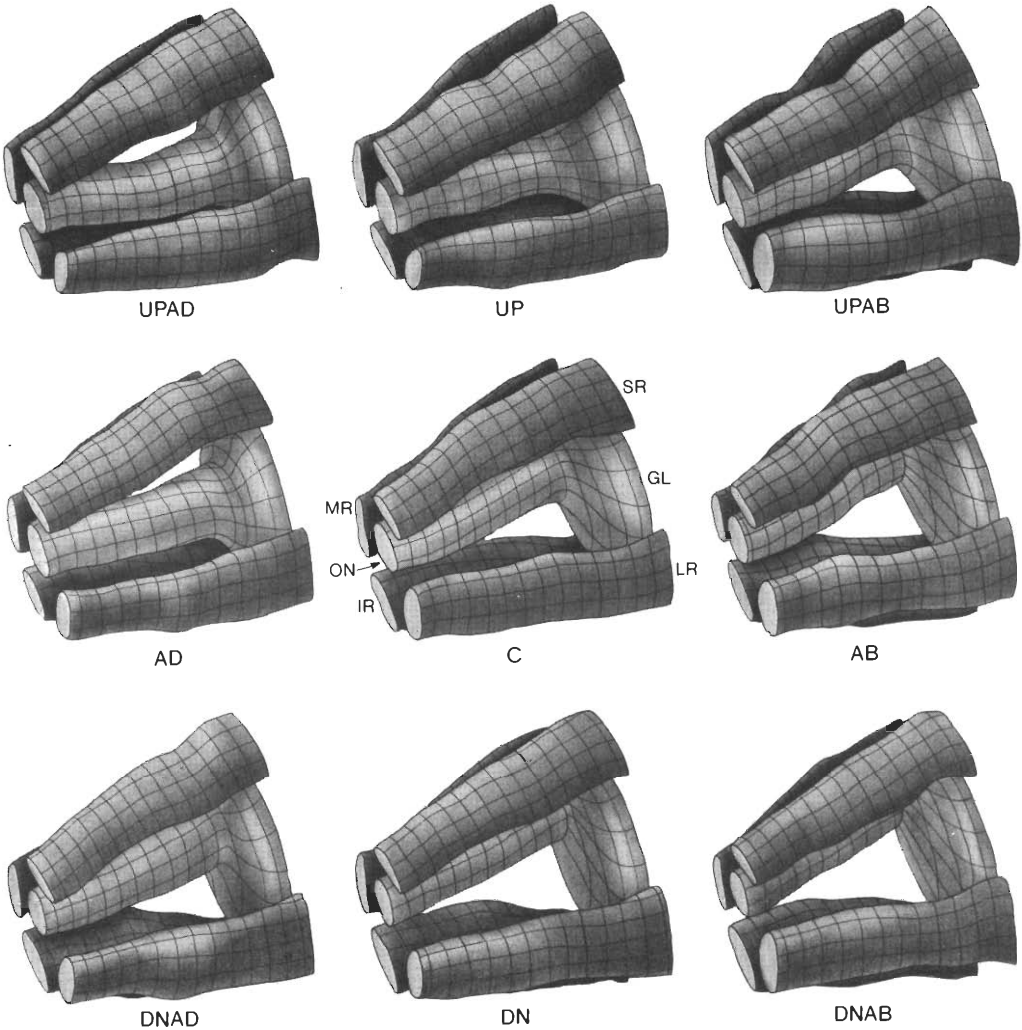

Fig. 7(B)

Fig. 7. Three-dimensional reconstructions of orbital contents. (A) Posterior-lateral-superior view of a right eye. (B) Posterior-medial-inferior view of a right eye. The lateral rectus (LR), medial rectus (MR), superior rectus (SR), inferior rectus (IR), optic nerve (ON), and a posterior portion of the globe (GL) are shown. At gaze position *C* the eye is aligned with the orbital axis; each of the other gaze positions is 38 deg eccentric from *C*, as shown in Fig. 2. The clearest indication of change in gaze position is the change in position of the optic nerve. The muscles can also be seen to thicken in their fields of gaze; see, e.g. the LR, as the eye moves from *AD* to *C* to *AB*. There is little evidence of sideways movement (side-slip). Each reconstruction reflects the data of all subjects, as described in the text.

The LR can be seen in side view in Fig. 5A, in the nine gaze positions described in Fig. 2. The sideways* stability of the LR over large vertical gaze changes is striking: whether the eye rotates from DN to UP (77 deg), DNAD to UPAD (52 deg) or DNAB to UPAB (52 deg), the LR shows almost no sideways movement. For all three vertical excursions there is a slight tendency for our most forward slice of LR to slide *downward* with *upward* rotation of the eye (as though it were stuck to the globe), but this movement is a fraction of a mm. The MR is seen in side view in Fig. 5B. It too is quite stable with respect to sideways movement. If we examine the vertical recti under horizontal gaze changes (Figs 5C and 5D: DNAD to DNAB [52 deg], AD to AB [77 deg], UPAD to UPAB [52 deg]) we again find no consistent sideways movements.

Figure 6 presents the centroid data in a form that exhibits the radial motion of the muscles, i.e. whether the muscles move towards or away from the orbital axis as the eye rotates (see Fig. 1B). The muscles all tend to move closer to the orbital axis when they contract, and away when they relax. The effect is largest for the SR (whose movements are as large as 3.7 mm), smallest for the IR (a maximum of 1.5 mm), and intermediate for the LR and MR (a maximum of 2.1 mm).

The effect is reasonably consistent. For each muscle, 23 comparisons are available, as above. The displacements are clearly seen in 17 out of the 23 comparisons for the LR, in 16 for the MR, in 22 for the SR, and in 16 for the IR.

Images of the orbital contents

The 3-dimensional reconstructions based on the data of all four subjects are shown in Fig. 7. Figure 7A views the data from a posterior-lateral-superior direction, which places the SR and LR in the foreground; Fig. 7B shows the same data from a posterior-medial-inferior direction, which places the MR and IR in the foreground. These figures serve as a visual summary of the relative magnitudes of the effects discussed above.

By far the largest effect of gaze on these images is seen in the position of the optic nerve; all other changes in the orbital contents are small by comparison.

*As defined above, "sideways" or "side-slipping" movement of the LR is vertical movement in Fig. 5A.

The effects of horizontal gaze changes on the LR and MR are easily seen in Figs 7A and 7B, respectively: in up, level, and down gaze, the LR can be seen to thicken and its point of maximum cross-section move posteriorly as the eye abducts; similar effects can be seen for the MR as the eye adducts. (Recall that the UPAB images are less reliable than the others, being based on the data of only 3 subjects.) Considering "vertical" gaze changes in Figs 7A and 7B, neither muscle appears to make significant sideways movements.

The changes in cross-section of the IR can be easily seen in Fig. 7B: for downward movements in both adduction and abduction the IR thickens and the point of maximum cross-section moves posteriorly. For the downward movements through central gaze, the thickening is apparent, but the posterior movement is not, as we would expect from the data of Fig. 4C. "Horizontal" gaze changes are accompanied by no apparent side-slip of the IR.

The radial displacements of the rectus muscles are, as one might expect, too small to be seen in Fig. 7.

DISCUSSION

Cross-sectional areas

Extant studies of orbital anatomy deal with fixed tissue. The most comparable data are those of Nakagawa (1965), although it should be noted that Nakagawa used fixed oriental orbits, while we studied live occidental subjects. Nakagawa provided data on the maximum cross-sections of rectus muscles, which we have converted to the slice orientation of the present study, for purposes of comparison (Table 1). The eyes abduct a few degrees in death so,

Table 1. Maximum cross-sectional areas of rectus muscles from serial sections of fixed orbits. Nakagawa (1965) sliced the orbits of 19 Japanese cadavers in frontal planes 5 mm apart. In his Figs 3 and 4 and associated tables, he presents the muscle areas. Here we give his maximum areas, adjusted for the difference in slice orientation (estimated to be 26 deg about a superior-inferior axis)

Muscle	Max area (mm^2)
LR	37.6
MR	34.4
SR	21.6
IR	28.0

perhaps, the best comparison with Nakagawa's data is provided by the average of our maximum area data for the AD and C gaze positions (see Fig. 4). Accordingly, we find the following: for the LR, a maximum cross-sectional area of 32.3 compared to Nakagawa's 37.6 mm^2; for the MR, 30.3 compared to 34.4 mm^2; for the IR, 33.6 compared to 28.0 mm^2. Thus, our values are similar to values derived from direct anatomic measurement; the MRI method does not appear to systematically underestimate or overestimate muscle cross-sections.

Radial movement of the muscle path

We found, as did Simonsz *et al.* (1985), that an agonist rectus mucle tends to straighten, moving radially inward, and an antagonist tends to curve radially outward. Simonsz *et al.* proposed that this might be due to pressure in the fat contained within the muscle cone, and we agree that this is a reasonable hypothesis, assuming, however, that there are no mechanically significant musculo-orbital elasticities. The relatively limited radial movement of the IR (Fig. 6B) might be due to its enclosure in the suspensory ligament of Lockwood (see, e.g. von Noorden, 1980, pp. 49–50).

Side-slip, muscle planes and axes of rotation

If muscles always too great-circle paths across the globe, we would have seen considerable side-slip, given the large globe rotations in the present study. Table 2 gives the side-slip values predicted by the "shortest-path hypothesis". The range of sideways movement would have been about 8 mm for the LR, 17 mm for the MR, 12 mm for the SR, and 14 mm for the IR. Instead, we found, consistent with Simonsz *et al.* (1985), essentially no side-slip for the MR, SR and IR. For the LR, we found, consistent with Miller and Robins (1987), only a fraction of a mm of side-slip, and this was in a direction opposite to that predicted by the shortest path hypothesis.

Table 2. Sideways movements of points of tangency if muscles took great-circle paths. Values are theoretical, calculated with the SQUINT computer model of orbital statics (Miller and Robinson, 1984). Values for the horizontal recti are v components of the projections of the points of tangency onto the w-v plane (see Fig. 1). Values for the vertical recti are the u components of projections onto the w-u plane. All have been normalized to set side-slip for gaze poisiton C to 0.0

Gaze	Fick coords (deg) θ, ϕ	LR (mm)	MR (mm)	SR (mm)	IR (mm)
DNAD	(−3.2, −26.0)	−3.8	−2.4	−6.9	−0.7
DN	(26.0, −38.3)	−2.7	−6.3	−4.6	2.0
DNAB	(55.2, −26.0)	−0.6	−8.7	5.2	3.7
AD	(−12.3, 0.0)	0.4	−0.2	−3.8	−4.2
C	(26.0, 0.0)	0.0	0.0	0.0	0.0
AB	(64.3, 0.0)	−0.1	0.8	4.8	5.3
UPAD	(−3.2, 26.0)	4.1	2.6	−0.5	−7.4
UP	(26.0, 38.3)	2.7	6.1	2.0	−5.3
UPAB	(55.2, 26.0)	0.4	8.6	3.5	6.2

Muscle side-slip in a given position of gaze is determined by: (1) muscle tension, which tends to make each muscle slip sideways across the globe to take the shortest path; (2) forces exerted by intermuscular attachments of the muscle sheaths, which tend to reduce side-slip with respect to the globe; and (3) forces exerted by musculo-orbital attachments of the muscle sheaths, which tend to stabilize the muscle with respect to the orbital wall. Koornneef (1983) describes fascial bands connecting the muscle sheaths with the bony orbit, as well as with each other. His studies, however, were purely anatomic and do not describe the mechanical properties of the fascia.

If musculo-orbital coupling were relatively stiff, it might explain why the belly of a rectus muscle side-slips hardly at all with respect to the orbit. However, if intermuscular coupling were negligible the tendency of the LR's point of tangency to move up (with respect to the orbit) as the eye looks down, and down as the eye moves up, would be hard to explain. That is, muscle tension would tend to make the muscle take the shortest path, and musculo-orbital attachments could only reduce, but not reverse, side-slip relative to the orbit. Because the point of tangency T (Fig. 1) lies posterior to the center of rotation, it is possible for intermuscular attachments to move it opposite to the direction of rotation.

Note that an appropriate combination of forces "1" and "2" (see above) could result in similar orbit-relative side-slip as that from a combination of forces "1" and "3". Thus, the data allows a model that includes significant intermuscular and musculo-orbital forces. In up-gaze, for example, the horizontal recti would tend to slip upward because of their tension. Intermuscular attachments would tend to reduce this globe-relative side-slip by coupling the muscles to the globe. A balance of these two forces might approximately fix T in the orbit. Direct coupling of the muscles to the orbit would serve to further stabilize them with respect to the orbit.

If the point of tangency T is fixed in the orbit, and the center of rotation of the globe is assumed to be fixed, then the rectus muscle planes are fixed with respect to the orbit. However, the action of a muscle is described by the axis of rotation (or *unit moment vector*), about which the eye tends to turn when the muscle contracts. The relationship between the axis of rotation and the muscle plane depends on the manner in which the muscles are stabilized with respect to the orbit. We conceive of two sorts of models that are consistent with experimental findings. Both suppose that the intermuscular fascia forms a sort of "harness" that effectively couples the muscle sheaths to the anterior hemisphere of the globe, thereby controlling globe-relative side-slip.

The first model supposes that, at and posterior to the u-v plane (which plane passes through the globe's center of rotation; see Fig. 1), the muscle sheaths function as a "pulley" fixed to the orbital wall. This arrangement would tend to make the axis of rotation move with the eye. Consider, for example, the LR. If gaze is straight ahead, clearly, the axis of rotation is vertical. However, if the eye rotates upward, bringing the LR insertion with it, and the fascial pulley remains fixed to the orbital wall, the axis of rotation will tip top-end-backwards in the orbit. Contraction of the LR will then no longer result in pure abduction, but rather in some combination of abduction, depression, and extortion. Note that, in a global, or retinotopic, coordinate system, the axis of rotation will remain fixed, and contraction of the LR will continue to rotate the eye along a horizontal retinal meridian.

The second model supposes that there is no pulley, indeed, no significant musculo-orbital coupling at all. According to this model, the anterior part of the LR, which bends upward in elevated gaze, has little mechanical import, since this part of the muscle is effectively fixed to the globe. The eye will behave as though the LR had a fixed insertion at a point on the globe lateral to the center of rotation, where the harness to the globe ends. Although the eye is elevated, the axis about which contraction of the LR tends to rotate the eye will remain vertical in the oribit.

If there were no pulley, and if the stiffness of the harness formed by the intermuscular tissues were low, then there might be enough globe-relative side-slip for a pair of antagonistic muscles to develop in certain gaze positions the cooperative action called the "bridle effect" (Robinson, 1975). For example, the horizontal recti might become elevators in up-gaze (or depressors in down-gaze). This would occur because their points of tangency T had slipped up (or down) relative to the center of rotation of the globe. The existence of a bridle effect would seem to make the brainstem's task of oculomotor control very difficult, leading some to propose that other effects cancel it. France and Burbank (1979) for instance, suggest that the nonuniform distribution of tension across the width of the muscle displaces the effective insertion enough to cancel the bridle force. However, the present results show that such a "no-pulley-soft-harness" model is wrong, and that, in normal eyes, there is no bridle force to cancel.

The "pulley" and "no-pulley" models require quite different eye movement control signals. For visual fixation, the pulley model allows the brain to deliver commands in retinotopic coordinates, independent of eye position in the head, while the no-pulley model requires that fixation commands take account of eye position. The opposite situation exists for the (nonvisual) vesibulo-ocular reflex. Compensatory VOR-movements of a no-pulley eye can be performed without changing the central commands to allow for gaze-dependent changes in eye muscle kinematics. Consider, for instance, a downward movement of the head in the plane of the left anterior and right posterior semicircular canals, and the compensatory movement of the left eye. In extreme adduction, the required intorsion would be supplied by the vertical recti alone. In extreme abduction, the required elevation would be supplied by the same muscle pair (see e.g. Simpson and Graf, 1985, pp. 10–11). Thus, the VOR could (at least roughly) stabilize a no-pulley eye in space without knowing its position in the head. In contrast, the VOR would have to take account of eye position in the head to stabilize a pulley eye.

If the pulley model is correct, muscle transposition surgery that does not reposition the pulley (i.e. the muscle sheaths adherent to the orbital wall) will not greatly change muscle actions. If, instead, the no-pulley model is correct, only anterior intermuscular tissues must be severed to achieve a large transposition effect. Consider the following extreme case, which makes the difference clear: imagine that we disinsert an LR, cut its (anterior) intermuscular membranes, and transpose it upward to the

insertion of the SR. The pulley model would predict that the LR would become primarily a excyclotorter, the pulley having remained fixed to its pre-surgical position on the orbital wall. In contrast, the no-pulley model would predict that the LR would swing around to follow a path similar to that of the SR and, thus, would become primarily an elevator. In fact, computer modeling (Miller and Robinson, 1984) suggests that transposition surgery produces an effect somewhere between that expected under the two models. The pulley model is further supported by our preliminary MRI studies of strabismus patients, before and after transposition surgery: the position of the belly of the LR and MR appears unaffected by transpositions of about 6 mm.

We have considered the pulley and no-pulley models in their strong forms for clarity. More plausible, intermediate models can be generated by considering pulleys with elastic connections to the orbital wall.

Acknowledgements—The author thanks Dr Kirk L. Moon, Jr of the Department of Radiology, Pacific Presbyterian Medical Center, San Francisco, for his enthusiastic and expert help with MRI and Dr Huibert J. Simonsz of the Klinikum der Albert Ludwigs Universitat, West Germany for his valuable remarks on a peliminary version of the manuscript. Bruce K. Smith wrote the digitizing software and adapted the Unigrafix package for our use, and Jim Brodale did the artwork. This study was supported by Grant EY06973 from the National Eye Institute, National Institutes of Health, Bethesda, Maryland, by Core Facilities Grant EY06883, and by the Smith-Kettlewell Eye Research Foundation.

REFERENCES

Boeder P. (1962) Co-operative action of extraocular muscles. *Br. J. Ophthal.* **46,** 397–403.

Bradley W. G. (1982) *NMR Tomography*. Diasonics, Milpitas, CA.

France T. D. and Burbank D. P. (1979) Clinical applications of a computer-assisted eye model. *Trans. Am. Acad. Ophthal. Otol.* **86,** 1407–1412.

Kault D. A., Stark D. J. and Stark K. P. (1987) Further investigations of a strabismus model. *Aust. N.Z. J. Ophthal.* **15**(1), 43–55.

Koornneef L. (1983) Orbital Connective Tissue. In: *Biomedical Foundations of Ophthalmology*, Vol. 1, Chapt. 32 (Edited by Duane T. D. and Jaeger E. H.). Harper & Row, Philadelphia.

Krewson W. E. (1950) The action of the extraocular muscles; a method of vector analysis with computations. *Trans. Am. Ophthal. Soc.* **48,** 443–486.

Mackay R. S. (1984) *Medical Images and Displays*. Wiley, New York.

Miller J. M. and Robins D. (1987) Extraocular muscle side-slip and orbital geometry in monkeys. *Vision Res.* **27**(3), 381–392.

Miller J. M. and Robinson D. A. (1984) A model of the mechanics of binocular alignment. *Comput. Biomed. Res.* **17,** 436–470.

Nakagawa T. (1965) Topographic anatomical studies on the orbit and its contents. *Acta Soc. Ophth. Jap.* **69,** 2155–2179.

von Noorden G. K. (1980) *Binocular Vision and Ocular Motility: Theory and Management of Strabismus*, 2nd edn. Mosby, St Louis.

Robinson D. A. (1975) A quantitative analysis of extraocular muscle cooperation and squint. *Invest. Ophthal.* **14,** 801–825.

Robinson D. A. (1985) Bielschowsky head-tilt test—II. Quantitative mechanics of the Bielschowsky head-tilt test. *Vision Res.* **25**(12), 1983–1988.

Saunders R. A., Croley T. L., Croley M. R. and Holgate R. C. (1986) The relationship of rectus muscles to the globe: a study with coronal CT scanning. *J. Pediat. Ophthal. Strabismus* **23,** 178–182.

Scott A. B. (1983) Ocular motility. In: *Biomedical Foundations of Ophthalmology*, Chap. 23. Harper & Row, Philadelphia.

Séquin C. H. (1983) Unigrafix. *IEEE 1983 Proc. 20th Design Automation Conf.*, 374–381.

Simonsz H. J., Harting F., de Waal B. J. and Verbeeten B. W. (1985) Sideways displacement and curved path of recti eye muscles. *Arch. Ophthal.* **103**(1), 124–128.

Simpson J. I. and Graf W. (1985) The selection of reference frames by nature and its investigators. In: *Adaptive Mechanisms in Gaze Control*, Chap. 1 (Edited by Berthoz A. and Melvill Jones G.). Elsevier, Amsterdam.

Volkmann A. W. (1869) Uber die mechanika der augenmuskeln. *Ber. Verh. Sächs. Acad. Wiss.* **21,** 28–69.